

**Title Page**

**Mitochondria, Calcium, and Calpain are Key Mediators of Resveratrol-  
Induced Apoptosis in Breast Cancer\***

Dhruv Sareen, Soesiawati R. Darjatmoko, Daniel M. Albert and Arthur S. Polans<sup>1</sup>

Department of Biomolecular Chemistry (D.S., A.S.P.),  
Department of Ophthalmology and Visual Sciences (D.S., S.R.D., D.M.A., A.S.P.), and  
the Paul P. Carbone Comprehensive Cancer Center (D.M.A., A.S.P.),  
University of Wisconsin School of Medicine and Public Health,  
Madison, Wisconsin 53792

**Running Title:** Mitochondria and calcium mediate resveratrol-induced apoptosis

**<sup>1</sup>Corresponding Author:** Arthur S. Polans, Ph.D., Department of Ophthalmology and Visual Sciences, School of Medicine and Public Health, Rm. K6/466 Clinical Sciences Center, 600 Highland Avenue, Madison, WI – 53792. Phone: (608) 265-4423; Fax: (608) 265-6021; E-mail: [apolans@wisc.edu](mailto:apolans@wisc.edu).

Number of text pages: 26

Number of Tables: 1

Number of Figures: 8

Number of References: 40

Number of words in Abstract: 249

Number of words in Introduction: 776

Number of words in Discussion: 1231

### **Abbreviations**

Smac/DIABLO, second mitochondria-derived activator of caspases/direct IAP binding protein with low pI; JC-1, 5,5',6,6'-tetrachloro-1,1',3,3'-tetraethylbenzamidazolocarboxyanin iodide; FCCP, carbonyl cyanide-p-(trifluoromethoxy)phenylhydrazone; BAPTA-AM; 1,2-bis(o-aminophenoxy)ethane-N,N,N',N'-tetraacetic acid-acetoxymethyl ester; S-LLVY-AMC, succinyl-Leu-Leu-Val-Tyr-7-amino-4-methylcoumarin; Ac-LEHD-AFC, N-acetyl-Leu-Glu-His-Asp-7-amino-4-trifluoromethylcoumarin; Ac-DEVD-AMC, N-acetyl-Asp-Glu-Val-Asp-7-amino-4-methylcoumarin; Z-VDVAD-AFC, benzyloxycarbonyl-Val-Asp-Val-Ala-Asp-7-amino-4-trifluoromethylcoumarin; Z-IETD-AFC, benzyloxycarbonyl-Ile-Glu-Thr-Asp-Asp-7-amino-4-trifluoromethyl coumarin.

## Abstract

Resveratrol (RES), a natural plant polyphenol, has gained interest as a non-toxic chemopreventive agent capable of inducing tumor cell death in a variety of cancer types. However, the early molecular mechanisms of RES-induced apoptosis are not well defined. Using the human breast cancer cell lines MDA-MB-231 and MCF-7, we demonstrate that RES is anti-proliferative and induces apoptosis in a concentration- and time-dependent manner. Preceding apoptosis, RES instigates a rapid dissipation of mitochondrial membrane potential ( $\Delta\Psi_m$ ) by directly targeting mitochondria. This is followed by release of cytochrome *c* and Smac/DIABLO into the cytoplasm and substantial increase in the activities of caspases-9 and -3 in MDA-MB-231 cells. Additionally, live cell microscopy demonstrates that RES causes an early biphasic increase in the concentration of free intracellular calcium ( $[Ca^{2+}]_i$ ), likely resulting from depletion of the endoplasmic reticulum (ER) stores in breast cancer cells. In caspase-3 deficient MCF-7 cells apoptosis is mediated by the  $Ca^{2+}$ -activated protease, calpain, leading to the degradation of plasma membrane  $Ca^{2+}$ -ATPase isoform 1 (PMCA1) and fodrin; the degradation is attenuated by buffering  $[Ca^{2+}]_i$  and blocked by calpain inhibitors. Mitochondrial permeability transition pore antagonists also blocked calpain activation. *In vivo* mouse xenograft studies demonstrate that RES treatment inhibits breast cancer growth with no systemic toxicities. Collectively, these results suggest a critical role for mitochondria not only in the intrinsic apoptotic pathway but also in the  $Ca^{2+}$  and calpain-dependent cell death initiated by RES. Thus, RES may prove useful as a non-toxic alternative for breast cancer treatment.

## Introduction

Despite earlier diagnosis and aggressive therapeutics, breast cancer remains a leading cause of death among women. The chance of developing invasive breast cancer during a woman's lifetime is approximately 1 in 8 and greater than 40000 women die of metastatic disease each year (Jemal, et al., 2006). Inherent or acquired tumor drug resistance limits many agents used in the treatment of this disease. In addition, these cytotoxic agents are often associated with severe, dose-limiting, systemic toxicities. Therefore, the need for development of novel non-toxic therapeutic agents active against breast cancer remains an important goal.

Basic and preclinical research on resveratrol (*trans*-3,4',5-trihydroxystilbene, RES), a naturally occurring polyphenol enriched in grapes and red wine, has shown pleiotropic cardioprotective, antiaging, and anticancer activities (Aggarwal, et al., 2004; Bradamante, et al., 2004; Savouret and Quesne, 2002). RES has been shown to inhibit tumor initiation, promotion, and progression in a variety of cell culture systems, including breast cancer cells (Bhat, et al., 2001; Jang, et al., 1997). Importantly, RES suppresses *in vivo* tumor growth in xenograft and mutagen-induced animal models of mammary carcinogenesis (Banerjee, et al., 2002; Garvin, et al., 2006). Preliminary studies in our laboratory suggest that RES is effective in preventing tumor growth in neuroblastoma and uveal melanoma murine xenograft models. Nevertheless, the precise mechanisms by which RES confers inhibition of tumor growth *in vivo* have not been well elucidated. *In vitro* studies on human cancer cell lines revealed that RES initiates anti-proliferative and/or pro-apoptotic actions (Savouret and Quesne, 2002). Recently, the pro-apoptotic effect of RES has been attributed to downstream events activated after binding to

putative cell surface receptors, including integrin  $\alpha V\beta 3$  and sulfonyleurea receptor isoform 1 (Hambrock, et al., 2007; Lin, et al., 2006). In addition, RES targets several enzymes involved in carcinogenesis, suggesting that multiple signaling cascades may be activated or inhibited depending on the cellular background (Sareen, et al., 2006).

Apoptosis requires the participation of intracellular zymogens that systematically dismantle the cell via two distinct pathways. Activated caspase-8 (extrinsic death-receptor pathway) and activated caspase-9 (intrinsic mitochondrial pathway) both activate the executioner caspase-3, which in turn activates the degradation phase of apoptosis (Ashkenazi and Dixit, 1998; Green and Reed, 1998). There is evidence that RES can induce apoptosis through both mechanisms, although the absence of functional caspase-3 in MCF-7 breast cancer cells indicates that alternative mechanisms may be involved (Delmas, et al., 2003; Mohan, et al., 2006; Sareen, et al., 2006). In a separate intrinsic apoptotic pathway, alterations in  $Ca^{2+}$  homeostasis involving the ER can cause a stress response. In resting cells, the concentration of  $Ca^{2+}$  in the extracellular milieu and in the ER is relatively high (in the mM range). In contrast, the cytoplasmic  $Ca^{2+}$  concentration is maintained at ~100 nM by active extrusion from the cell by plasma membrane  $Ca^{2+}$ -ATPases (PMCA), plasma membrane  $Na^+/Ca^{2+}$  exchangers (NCX), and active uptake of cytosolic  $Ca^{2+}$  into the ER and mitochondria by distinct  $Ca^{2+}$ -ATPases and transporters, respectively. During elevated levels of cytosolic  $Ca^{2+}$  the mitochondrial membrane potential ( $\Delta\Psi_m$ ) drives  $Ca^{2+}$  uptake into the mitochondria. Under conditions of stress, de-energized mitochondria release  $Ca^{2+}$  back to the cytosol via different mechanisms, opening of the mitochondrial permeability transition pore (mPTP) being one (Orrenius, et al., 2003). Loss of  $Ca^{2+}$  homeostatic

control either by release from the ER and mitochondria or influx through plasma membrane channels leads to sustained levels of cytosolic  $\text{Ca}^{2+}$  and cell death. However, the mechanisms that couple changes in cellular  $\text{Ca}^{2+}$  to apoptotic cell death in response to RES have been elusive and, particularly, the apoptosis related  $\text{Ca}^{2+}$  targets have not been identified.

While the best characterized proteases in apoptosis are caspases, other proteases including calpains and cathepsins contribute to apoptosis in the absence of caspase activation (Harwood, et al., 2005). The  $\text{Ca}^{2+}$ -dependent cysteine proteases, m- and  $\mu$ -calpains, are frequently activated in apoptosis models involving elevated  $[\text{Ca}^{2+}]_i$ . Calpain substrates include membrane receptors and transporters, cytoskeletal proteins, and intracellular enzymes. In particular, there is evidence that proteolysis of NCX3 by calpain plays a prominent role in the delayed and irreversible  $\text{Ca}^{2+}$  elevation leading to neuronal demise (Bano, et al., 2005). However, the mechanisms of cellular calpain activation during apoptosis are not well understood, and little is known about the involvement of calpains in tumor cell death.

In this study, we sought to investigate the early and pivotal intracellular apoptotic signaling mechanisms in MDA-MB-231 (caspase-3 positive) and MCF-7 (caspase-3 negative) breast cancer cells in response to RES. We demonstrate that RES significantly inhibits tumor growth in a xenograft model of breast cancer. *In vitro* and *in vivo* data show that RES induces mitochondrial depolarization and a transient spike in  $[\text{Ca}^{2+}]_i$ , followed by a secondary gradual rise in  $[\text{Ca}^{2+}]_i$  contributing to an irreversible commitment to undergo the execution phase mediated by caspases and calpains. We show that the intrinsic mitochondrial caspase-dependent apoptotic pathway is activated

in MDA-MB-231 cells. In addition to this caspase-dependent pathway, elevated  $[Ca^{2+}]_i$  is induced by RES in both MDA-MB-231 and MCF-7 cell lines. This leads to activation of calpain and the subsequent proteolysis of *in vivo* substrates, including fodrin and PMCA1. These latter events are more readily observed in the caspase-deficient MCF-7 cells.

## Materials and Methods

**Materials.** The human breast cancer MCF-7 and MDA-MB-231 cell lines were obtained from Dr. Elaine Alarid (University of Wisconsin, Madison, WI). RES purchased from Cayman Chemicals (Ann Arbor, MI) was dissolved in sterile DMSO and further diluted in cell culture media. Mouse monoclonal antibodies were purchased for GAPDH from Biogenesis Inc (Poole, UK), cytochrome oxidase subunit IV (clone 12C4) from Molecular Probes (Eugene, OR), cytochrome c (clone 7H8.2C12) from BD PharMingen (San Diego CA), Smac/DIABLO from Cell Signaling Technology (Danvers, MA),  $\alpha$ -fodrin (clone AA6) from BIOMOL International LP (Plymouth Meeting, PA), AIF (E-1) from Santa Cruz Biotechnology (Santa Cruz, CA). Rabbit polyclonal PMCA1 antibody was obtained from Affinity Bioreagents (Golden, CO). All other common reagents were procured from SIGMA Chemical Co. (St. Louis, MO).

**Cell Culture.** MDA-MB-231 and MCF-7 cells were grown in Dulbecco's modified eagle medium, supplemented with 10% v/v fetal bovine serum, 2 mM L-glutamine, 100 units/ml penicillin G, 100 mg/ml streptomycin sulfate and 0.25 mg/ml amphotericin B. Cultures were maintained at 37°C in 95% O<sub>2</sub>/5% CO<sub>2</sub>.

**Breast Cancer Xenograft Study.** Female athymic *nu/nu* mice, ~6 weeks of age (Harlan Sprague Dawley, Indianapolis, IN), were housed in a pathogen-free isolation facility. Animal care and treatment protocols were approved by the University of Wisconsin-Madison Research Animals Resources Center. MDA-MB-231 cells were harvested, 5 X10<sup>6</sup> cells resuspended in 500  $\mu$ l of 1:1 culture media and basement membrane matrix (Matrigel; BD Biosciences, Bedford, MA) and injected subcutaneously into the dorsal flanks of seventy-two mice. After the tumors were established (150 mm<sup>3</sup>),



the animals were randomized into control and treatment groups (n = 36 mice per group). Control group animals were administered 0.1 ml Neobee M5 oil alone, and treatment group animals received 50 mg/kg resveratrol in 0.1 ml Neobee M5 oil by oral gavage daily for five weeks. Twice weekly during the treatment each animal was weighed and the tumor volume was determined by measuring tumor size in three dimensions using calipers. Toxicity was assessed by survival, activity and changes in body weight. At the completion of five weeks of treatment, the mice were euthanized, tumors, lungs and livers fixed in 10% neutral buffered formalin for histopathologic processing. Five-micrometer sections were cut and stained with hematoxylin–eosin (H&E) for light microscopic analysis.

**Tumor Cell Viability.** MCF-7 and MDA-MB-231 cells were seeded in 96-well plates for 2 days and incubated with either DMSO or RES for a period of 1 to 7 days. At the end of the treatment CellTiter-Blue™ dye was added according to the manufacturer's instructions (Promega, Madison, WI). Fluorescence was measured at excitation/emission wavelengths of 560/590 nm, using a fluorescence plate reader (Molecular Dynamics, Sunnyvale, CA).

**Cell Cycle Distribution Analysis.** Propidium iodide (PI) staining was used to analyze DNA content on a flow cytometer (Becton Dickinson; FACStation) equipped with cell cycle analysis software, using standard procedures (Sareen, et al., 2006).

**Determination of Apoptotic Cell Morphology.** MCF-7 and MDA-MB-231 cells were seeded into 8-well LabTek II chamberslides (Nalge Nunc International, Naperville, IL) and treated with 100  $\mu$ M RES. At the end of the treatment cells were fixed, washed, and stained with 1  $\mu$ g/ml Hoechst 33528 (Molecular Probes), using standard procedures

(Sareen, et al., 2006). Cells were viewed under a fluorescence microscope (Carl Zeiss, Oberkochen, Germany) using a DAPI filter set and apoptotic cells counted.

**Isolation of Mitochondria.** Mitochondria from MCF-7 and MDA-MB-231 cells were isolated using a Potter-Elvehjem homogenizer according to previously published methods (Sareen, et al., 2006).

**Mitochondrial Transmembrane Potential ( $\Delta\Psi_m$ ).** Changes in mitochondrial membrane potential from whole cells and isolated mitochondria were analyzed on a Shimadzu RP 5301-PC spectrofluorometer (Shimadzu Scientific, Columbia, MD) using the mitochondria-selective dye, JC-1 (Cell Technology, Mountain View, CA), as described previously (Sareen, et al., 2006).

**Cytochrome c and Smac/DIABLO Release.** Cytosolic and mitochondrial extracts were analyzed for cytochrome c and Smac/DIABLO content by immunoblotting, as described previously (Pozo-Guisado, et al., 2005; Sareen, et al., 2006). Protein concentration of the fractions was determined using the Bio-Rad protein assay kit (Bio-Rad, Hercules, CA). Purity of the cytosolic fraction was confirmed by immunostaining with a mitochondrial specific marker, cytochrome oxidase subunit IV. GAPDH, a cytoplasmic protein, served as a control for protein loading.

**Determination of Caspase Activation.** MCF-7 and MDA-MB-231 cells were seeded on 10 cm culture dishes, treated with either vehicle, RES, additional apoptotic stimuli, and the activities of caspases-2, 3, 8, and 9 determined as previously described (Mohan, et al., 2006; Sareen, et al., 2006). Briefly, at the end of treatment cells were sedimented and resuspended in lysis buffer (10 mM Tris-HCl, 10 mM NaH<sub>2</sub>PO<sub>4</sub>, pH 7.5, 130 mM NaCl, 1% (v/v) Triton X-100) and protein concentration measured (Bio-Rad).

Subsequently, incubation of 80  $\mu\text{g}$  protein with caspase-9 substrate (Ac-LEHD-AFC; MP Biomedicals, Irvine, CA), 40  $\mu\text{g}$  protein with caspase-3 substrate (Ac-DEVD-AMC; BD PharMingen), 100  $\mu\text{g}$  protein with caspase-2 substrate (Z-VDVAD-AFC; EMD Biosciences), or 100  $\mu\text{g}$  protein with caspase-8 substrate (Z-IETD-AFC; EMD Biosciences) was performed in reaction buffer (100 mM HEPES, 1 mM EDTA, pH 7.1, 0.1% CHAPS, 10 % glycerol, 20 mM DTT) for 60 min at 37°C. Fluorescence of free AFC and AMC was monitored on a spectrofluorometer at excitation/emission wavelengths of 400 nm/505 nm and 380 nm/440 nm, respectively.

**Intracellular Calcium Imaging.** Changes in  $[\text{Ca}^{2+}]_i$  were assessed using the cell permeant  $\text{Ca}^{2+}$ -sensitive ratiometric fluorescent indicator dye, fura-2-AM (Molecular Probes), as described previously (Robinson, et al., 2004). Briefly, MCF-7 and MDA-MB-231 cells seeded in 96-well imaging plates (BD Biosciences, San Jose, CA) were rinsed twice in buffer (5.9 mM KCl, 1.4 mM  $\text{MgCl}_2$ , 10 mM HEPES, 1.2 mM  $\text{NaH}_2\text{PO}_4$ , 5 mM  $\text{NaHCO}_3$ , 140 mM NaCl, 11.5 mM glucose, 1.8 mM  $\text{CaCl}_2$  and 3 mg/ml bovine serum albumin (BSA), pH 7.3) and loaded with 8  $\mu\text{M}$  fura-2 AM in loading buffer at 37 °C for 30 min. Following 30 min RT incubation to allow for hydrolysis of the AM-ester, cells were rinsed in physiological salt solution (PSS), comprised of loading buffer lacking BSA. BAPTA-AM (20  $\mu\text{M}$ ; EMD Biosciences, San Diego, CA) was co-loaded with fura-2-AM where indicated. Dilutions of RES, TG and DMSO were made in PSS. Serial acquisition of fluorescent images of cells were performed in a non-confocal mode on a BD Pathway™ Bioimager system (BD Biosciences Bioimaging Systems, Rockville, MD), equipped with a temperature and  $\text{CO}_2$  regulated environmental chamber, a liquid handling single-channel pipettor with image-as-you-add capabilities, and a 20X plan-

fluorite objective (20X LUC Plan FLN, NA 0.45; Olympus, Japan). Fura-2-AM was alternately excited at wavelengths of 340 and 380 nm, and emitted fluorescence was collected via a 510 nm band pass filter at each UV wavelength with an internal high resolution Hamamatsu ORCA ER cooled CCD camera (Hamamatsu Photonics, Japan). Basal images were collected for 25 s before drug addition. Subsequently, images were collected after the indicated treatments at 2.5 s intervals.  $[Ca^{2+}]_i$  maps for individual cells were calculated after pixel-by-pixel computerized ratiometric reconstruction of individual images acquired using Attovision 5.0 3D imaging software. Calibration of the fluorescent signal was performed with fura-2 penta- $K^+$  salt using the two-point calibration procedure of imaging positive (10  $\mu$ M fura-2 + 1 mM  $CaCl_2$ ) and negative (10  $\mu$ M fura-2 + 1 mM EGTA-Na) calcium standards. Software assisted ratio to  $[Ca^{2+}]_i$  transformation was performed using the Grynkiewicz equation (Grynkiewicz, et al., 1985).

**Calpain Activity.** Calpain activity in intact cells was monitored using a Shimadzu RP 5301-PC spectrofluorometer (Shimadzu Scientific, Columbia, MD) by measuring  $Ca^{2+}$ -dependent and calpain specific hydrolysis of the peptidyl 7-amino bond of the cell-permeable fluorogenic calpain substrate, S-LLVY-AMC (Sigma) (Potter, et al., 1998). Previous studies have demonstrated that this assay is linear with cell number and the activity measured is representative of m- and  $\mu$ -calpain activities observed with protein substrates (Guttmann and Johnson, 1998; Sasaki, et al., 1984). Briefly, cells from confluent dishes were harvested with 0.25% trypsin-EDTA solution, neutralized with 10% fetal bovine serum containing media and washed twice with HEPES- buffered Hank's balanced salt solution (pH 7.4, without phenol red). Equal numbers of cells per assay were resuspended in HEPES-buffered Hank's balanced salt solution at  $2.5 \times 10^5$

cells/ml and pre-warmed at 37°C in a 5% CO<sub>2</sub> incubator for 10 min. Wherever indicated, the intracellular Ca<sup>2+</sup>-chelator BAPTA-AM (20 μM), the cell-permeable μ- and m-calpain inhibitors, PD 150606 (50 μM; selectively blocks the Ca<sup>2+</sup> binding sites), SJA 6017 (50 μM; active site inhibitor), and MDL 28170 (25 μM; active site inhibitor) and the mPTP inhibitor, cyclosporine A (20 μM) (EMD Biosciences), were pre-treated in the cell suspension, mixed and incubated at 37°C for 30-45 min. To assay calpain activity, RES (100 μM final concentration) or DMSO vehicle was added to untreated or pre-treated cell suspension (2.5 × 10<sup>5</sup> cells) 1 min prior to S-LLVY-AMC (25 μM) addition. AMC fluorescence was measured and calpain activity plots obtained at various time points on the spectrofluorometer with the excitation/emission wavelengths of 360 nm/400-500 nm. The initial rate of substrate cleavage, which was linear, was measured at 5-15 min post-substrate addition. Trypan blue exclusion was used to ensure that the cells remained viable through the procedure.

**Immunoblotting.** Cultures were washed twice with PBS and lysed in ice-cold lysis buffer [50 mM Tris-HCl (pH 7.5), 150 mM NaCl, 0.5% Nonidet P-40, 1 mM PMSF, 1 mM NaF, 1 mM DTT and 4 mg/ml complete protease inhibitor cocktail]. Protein concentration was determined in cell lysates using the Bio-Rad protein assay kit. Aliquots of protein were mixed with SDS sample buffer and Western blot analysis performed using standard protocols (Sareen, et al., 2006).

## Results

**Resveratrol Inhibits Tumor Growth in Athymic Nude Mice.** We examined the effect of resveratrol on human breast cancer tumor growth *in vivo* by ectopic implantation of MDA-MB-231 cells into athymic nude mice. After 5 weeks of oral drug treatment, tumor growth in the RES-fed group as compared to the control groups that were fed vehicle alone was inhibited by 51% ( $p = 0.003$ ) (Table 1). RES treatment had no effect on body weight and diet consumption during the 5 weeks of the experiment. No other signs of systemic toxicity or any adverse health effects as monitored by activity and posture of mice were observed. Furthermore, liver sections from RES-treated mice showed no evidence of abnormal pathology compared with those from controls. In addition, 14% (5/36) of the mice in the MDA-MB-231 RES-treated group showed regression of tumor size relative to the initial tumor volume (data not shown).

**Resveratrol Displays Dose- and Time-Dependent Pro-Apoptotic and Anti-Proliferative Effects in Breast Cancer Cells.** To examine the anti-tumor activity of RES in human breast cancer cells, exponentially dividing MDA-MB-231 and MCF-7 cells were treated with increasing concentrations of RES and cell viability was measured over time. RES caused marked growth inhibition and significantly decreased the viability of MDA-MB-231 cells ( $IC_{50}$  at 48 h = 128.8  $\mu$ M) and MCF-7 cells ( $IC_{50}$  at 48 h = 151.8  $\mu$ M) in a time- and concentration-dependent manner when compared with the DMSO treated control (Fig. 1A). At 100 to 200  $\mu$ M RES there was a regression in the number of viable cells (Fig. 1A; compare day 1 and day 7). The cytotoxicity caused by RES may in part be due to anti-proliferative and pro-apoptotic effects. Consequently, the effect of

RES on cell cycle progression was analyzed by flow cytometry in exponentially dividing cultures of MDA-MB-231 and MCF-7 cells treated with either DMSO or RES and the percentage of cells in G<sub>0</sub>/G<sub>1</sub>, S, and G<sub>2</sub>-M phase were calculated (Fig. 1B). RES caused an accumulation of cells in the S phase of the cell cycle for both cell lines, MDA-MB-231 (21% in control vs. 70% and 71 % with 50 and 100 μM RES, respectively) and MCF-7 (47% in control vs. 70% with 50 μM RES) with a concomitant decrease in the population of cells in the G<sub>0</sub>/G<sub>1</sub> phase, indicative of a late S phase or early G<sub>2</sub>-M block. Interestingly, at 100 μM RES the population of MCF-7 cells in G<sub>0</sub>/G<sub>1</sub> increased to 54% while cells in G<sub>2</sub>-M decreased to 2%, suggestive of an early S phase block. This data is consistent with previous observations from other groups (Aggarwal, et al., 2004; Kim, et al., 2004). The block in cell cycle progression, therefore, contributes to RES-induced anti-proliferative effects. In addition, there was a significant increase in the sub-G<sub>1</sub> fraction (hypodiploid DNA content) in both cell lines, possibly due to DNA fragmentation resulting in an increase in RES-induced apoptotic cell death (data not shown). Subsequently, the ability of RES to cause MDA-MB-231 and MCF-7 cell apoptosis was determined by examining nuclear morphological changes with fluorescence microscopy. Cells that exhibited typical morphological features of apoptosis such as chromatin condensation and pyknotic nuclei increased in a time-dependent manner when treated with RES. Results are represented as percent apoptotic cells, which increased from 1.3% and 0.9% in control to 52% and 45% in RES treated MDA-MB-231 and MCF-7 cells, respectively (Fig. 1C), suggesting that RES has a pro-apoptotic effect in both breast cancer cell lines. These morphological changes indicative of apoptotic cell death were further

confirmed by transmission electron microscopy (TEM) providing evidence that the mitochondria were predominantly affected by RES (data not shown).

**Resveratrol Disrupts Mitochondrial Function in Breast Cancer Cells.** During chemical induced apoptosis early and pivotal events occur in the mitochondria that are often, though not always, associated with the collapse in the mitochondrial membrane potential ( $\Delta\Psi_m$ ) (Sun, et al., 1999). To delineate this mechanism we measured RES-induced alterations in  $\Delta\Psi_m$  by utilizing the mitochondrial selective lipophilic cation JC-1. In MDA-MB-231 and MCF-7 cells, RES exerts a dose-dependent decrease in the ratio of JC-1 red-green fluorescence intensity after 10 minutes of treatment, representing cells with rapidly depolarized mitochondria (Fig. 2A and B). Significant depolarization with 2 – 10 fold decrease in  $\Delta\Psi_m$  can be observed in both cell lines after RES treatment. Positive controls, FCCP (protonophore) and valinomycin (potassium ionophore) function as uncouplers of mitochondrial oxidative phosphorylation and significantly dissipate electrochemical gradients across the inter-membrane space (IMS) (Fig. 2A and B). The RES-induced collapse of  $\Delta\Psi_m$  could either be due to its effects on mitochondrion stability through an indirect mechanism and/or direct interaction with the mitochondria.

We therefore determined whether RES might directly target mitochondria in a cell-free system to induce the collapse of  $\Delta\Psi_m$ . Freshly isolated mitochondria were incubated with JC-1 dye following treatment with various doses of RES and the intensity of red fluorescence was monitored, with a decrease signifying the inability of the dye to form J-aggregates (red) in the mitochondria due to a loss of  $\Delta\Psi_m$ . RES directly causes a concentration-dependent decrease in  $\Delta\Psi_m$  in the suspension of isolated mitochondria,



which is rapid (within 10 min) and irreversible after drug removal (Fig. 2C and D). In isolated mitochondria the changes in  $\Delta\Psi_m$  following RES treatment can be observed starting at considerably lower concentrations (Fig. 2C, compare with Fig. 2A), compared to whole cells. At 10  $\mu$ M RES, the J-aggregates are almost undetectable in the isolated mitochondria, indicating complete loss of  $\Delta\Psi_m$ . Positive controls, FCCP and Na-azide, which is an electron transport chain inhibitor, also significantly depolarize mitochondrial membranes. Thus RES causes mitochondrial dysfunction, likely through its ability to directly target the mitochondria.

**Resveratrol Mediates Release of Apoptogenic Factors from the Mitochondria of MDA-MB-231 cells.** Various apoptotic stimuli lead to changes in mitochondrial membrane permeability resulting in loss of  $\Delta\Psi_m$  and the subsequent release of apoptogenic factors, including cyt *c* and Smac/DIABLO. Western blot analysis was performed on cytosolic and mitochondrial fractions isolated from UNT or RES treated breast cancer cells. In MDA-MB-231 cells cyt *c* and Smac/DIABLO could be detected in the cytosolic compartment as early as 4h after RES exposure (Fig. 3). Both proteins are progressively released into the cytosolic fraction in increasing amounts over 4 – 48h of RES treatment, following a loss in  $\Delta\Psi_m$  seen much earlier at 15 min post-treatment. However, similar to our observation in other cancer models, RES could not provoke cyt *c* or Smac/DIABLO release from isolated mitochondria of breast cancer cells (data not shown), perhaps indicating a requirement for additional cytosolic factors (Sareen, et al., 2006).

**Resveratrol Activates Caspase-Dependent and -Independent Cell Death in MDA-MB-231 and MCF-7 Cells, Respectively.** Mitochondrion- and death receptor-dependent apoptosis is known to be executed by the linkage activation of initiator caspases, which include caspases-2, -8, -9, -10, and -12, and effector caspases, which include caspases-3, -6, and -7. We and others have established that loss of  $\Delta\Psi_m$  and release of apoptogenic factors accompanies mitochondrion-dependent apoptosis induced by RES (Aggarwal, et al., 2004; Sareen, et al., 2006). To further determine the involvement of caspases in breast cancer cells upon RES-induced  $Ca^{2+}$  deregulation and mitochondria mediated apoptosis, we examined cleavage of fluorogenic peptide substrates that mimic the target cleavage sites of caspases-2, -8, -9, and -3/7. It has been reported that MCF-7 cells lack caspase-3 activity due to a point mutation in the gene coding for this protein (Janicke, et al., 1998). As expected, RES was unable to induce caspase-3 as well as caspase-9 activation in this cell line (Fig. 4A and B). However, a demonstrable time-dependent increase in the activities of caspase-9 and -3 can be identified in RES treated MDA-MB-231 cells (Fig. 4A and B). Slight increase in caspase-9 and -3 activities were already detectable 24 h after the addition of RES, although maximum activation of ~3-5 fold was observed after 72 h.

RES-induced apoptosis also could be regulated by the death-receptor pathway via early caspase-2 and -8 activation (Mohan, et al., 2006). To address this possibility, cells were treated with RES and incubated with caspase-2 and -8 specific peptide substrates. RES was unable to induce either caspase-2 or -8 activation in MCF-7 and MDA-MB-231 cells when compared to the UNT control (Fig. 4C and D). This effect could not be attributed to MDA-MB-231 cells being refractory to activation of caspase-2 and -8 since

the apoptotic inducers, UV, TG, and staurosporine provoked significant activation of the proteases. Caspase-2 activation could not be detected in MCF-7 cells in response to any apoptotic stimuli tested. Moreover, we did not observe cleavage and activation of procaspase-12, an ER stress specific initiator caspase, upon RES treatment (data not shown).

**Resveratrol Increases Intracellular Calcium Levels in Breast Cancer Cells.** In many cases, an early and pivotal event in apoptosis is a  $\text{Ca}^{2+}$  influx through plasma membrane channels and/or release from the ER into the cytosol. Recently, RES has been demonstrated to enhance agonist-stimulated  $[\text{Ca}^{2+}]_i$  increase in endothelial cells of the heart valve, however, there is no information whether alteration of  $\text{Ca}^{2+}$  homeostasis plays a pivotal role during early RES-mediated cell death (Buluc and Demirel-Yilmaz, 2006). To determine if this was an early event during RES-induced apoptosis we first examined whether intracellular  $\text{Ca}^{2+}$  levels increased in log-phase MCF-7 cells after RES exposure utilizing fura-2-AM in a spectrofluorometric assay. Eight-min post treatment, RES and ionomycin cause a ~ 3-fold and 1.7-fold increase in  $[\text{Ca}^{2+}]_i$ , respectively, as compared to the vehicle control (Fig. 5A).

This result was substantiated by performing live cell  $\text{Ca}^{2+}$ -imaging on a BD Pathway Bioimaging™ microscopy system with fura-2 loaded MCF-7 cells. Before drug addition cells analyzed in different regions of interest (ROI) started with comparable basal fura-2 fluorescence, reflecting resting intracellular  $\text{Ca}^{2+}$  levels. After RES addition an elevation in intracellular  $\text{Ca}^{2+}$  levels was observed within different ROI of MCF-7 cells (Fig. 5B), supporting data from our spectrofluorometric assay. The same results were obtained

from similar experiments conducted with MDA-MB-231 cells. Figure 5 further illustrates the kinetics of RES-induced changes in  $[Ca^{2+}]_i$  and provides an indication of the source of  $Ca^{2+}$  release. The basal  $[Ca^{2+}]_i$  level in MDA-MB-231 cells was  $142 \pm 39$  (mean  $\pm$  SE) nM;  $n = 36$ . At 10 – 35s after exposure to RES, cells exhibited a significant spike of ~2-4 fold increase in  $[Ca^{2+}]_i$  with peak levels at  $476 \pm 96$  nM, after which time the levels returned to approximately  $283 \pm 44$  nM, although never reaching the basal levels (Fig. 5C; images with inset and graph). Interestingly, beginning at ~240 s after RES exposure there was a second gradual rise in  $[Ca^{2+}]_i$  that saturated at ~900 s with a peak value of  $422 \pm 68$  nM and did not return to resting levels within the experimental time of 45 min. The basal level of  $[Ca^{2+}]_i$  ( $128 \pm 29$  nM;  $n = 28$ ) was not affected significantly in both cell lines upon treatment with the DMSO vehicle control (Fig. 5E; top right panel). To ensure that the RES-induced changes in  $[Ca^{2+}]_i$  detected by fura-2 are  $Ca^{2+}$ -specific, cells pre-loaded with the intracellular  $Ca^{2+}$  chelator, BAPTA-AM, were evaluated by imaging. BAPTA-AM increased the cytosolic  $Ca^{2+}$  buffering capacity of the cells as the magnitude of the  $[Ca^{2+}]_i$  rise following RES exposure was almost completely attenuated (Fig. 5E; bottom right panel.) Untreated or BAPTA-AM-loaded cells did not show fluctuations in basal  $Ca^{2+}$  levels during the time course of the experiment.

Since the ER is a major intracellular reservoir of  $Ca^{2+}$ , we tested whether the  $Ca^{2+}$  signal evoked by RES originated from this organelle by employing TG, a known specific mobilizer of the ER  $Ca^{2+}$  stores causing rapid and transient increases in  $[Ca^{2+}]_i$ . If RES exposure led to release of  $Ca^{2+}$  stored in the ER then TG administration should not cause additional  $Ca^{2+}$  release. If the sequence of drug administration were reversed, additional  $Ca^{2+}$  release should not be observed. TG alone evoked a typical  $Ca^{2+}$

response of ~3-4 fold increase over basal  $[Ca^{2+}]_i$  35 s after exposure with cells reaching maximal concentration of  $454 \pm 82$  nM (Fig. 5D; images and graph). When TG was added to cells after RES, none of the cells that initially responded to RES exhibited a rise in intracellular  $Ca^{2+}$  levels subsequent to TG administration (Fig. 5E; bottom left panel). Similarly, when RES was added after TG-induced depletion of ER  $Ca^{2+}$  stores, no measurable spike was observed (Fig. 5E; top left panel). However, the second gradual rise in  $[Ca^{2+}]_i$  was unaffected by RES addition. We noted that the increase in  $[Ca^{2+}]_i$  (3-4-fold over basal levels, Fig. 5C) observed after exposure to RES was comparable to that elicited by TG (Fig. 5D), further suggesting that the two agents may mobilize the same ER pool of  $Ca^{2+}$ . The percentage of cells responding to RES and TG in a given culture was similar, averaging ~80%.

### **Resveratrol Activates a Calpain-Dependent Apoptotic Pathway in MCF-7 Cells.**

Despite the lesion in the intrinsic mitochondrial apoptotic pathway MCF-7 cells undergo apoptosis in response to RES at an  $IC_{50}$  similar to MDA-MB-231 cells that express caspase-3. The rise in  $[Ca^{2+}]_i$  and the resulting  $Ca^{2+}$  overload is thought to activate  $Ca^{2+}$ -dependant proteases, such as calpains, leading to structural damage and eventually cell death in certain neuronal models of apoptosis (Bano, et al., 2005; Liu, et al., 2004). However, to date little is known about the involvement of calpains in tumor cell death. To avoid the invasive procedure of cellular lysates, we performed the calpain activity assay in intact MCF-7 cells, by using a cell-permeable and fluorescent calpain substrate, S-LLVY-AMC. Additionally, MCF-7 cells provided an advantage to unmask a calpain-dependent apoptotic pathway due to the absence of an active caspase-

dependent intrinsic mitochondrial apoptotic pathway. Calpain activity in RES-treated cells is early and significantly higher compared to the basal levels observed in DMSO control treated cells, measured at 15 min post-drug addition (Fig. 6A). As expected, in samples pre-treated with the intracellular  $\text{Ca}^{2+}$ -chelator, BAPTA-AM, and calpain inhibitors with various specificities, PD 150606, MDL 28170, and SJA 6017, the RES-induced increase in calpain activity is almost completely blocked. This bolsters evidence that the fluorescent signal measured in this assay is dependent upon an increase in intracellular  $\text{Ca}^{2+}$  and is specific for calpain activity. The RES-induced increase in calpain activity remains substantial at 36 h post-treatment (data not shown).

Upon apoptotic insult, the mitochondria play an essential role in buffering non-toxic loads of  $\text{Ca}^{2+}$  and the mPTP provides a fast  $\text{Ca}^{2+}$  extrusion mechanism in response to abnormally high levels that accumulate in mitochondria during apoptosis. Some mPTP antagonists, like cyclosporine A (CsA), have been shown to inhibit this process, either through specific inhibition of cyclophilin D or through inhibition of calcineurin phosphatase activity (Montero, et al., 2004). To determine whether mitochondrial  $\text{Ca}^{2+}$  release from mPTP was involved in RES-induced calpain activation we employed the mPTP inhibitor, CsA. The increase in AMC fluorescence, indicating calpain activation, can be seen in RES-treated MCF-7 cells (Fig. 6B). Interestingly, RES-induced calpain activation was completely abolished by CsA pretreatment. The fact that CsA prevented calpain activation suggests that mPTP somehow mediates the observed calpain activation following RES treatment.

## Degradation of Calpain-Specific Protein Substrates Contributes to

**Resveratrol-Induced MCF-7 Cell Death.** To further characterize the mechanism of calpain-dependent cell death initiated by RES, we investigated the *in vivo* cleavage pattern of calpain protein substrates in MCF-7 cell lysates by Western analysis (Fig. 7). Fodrin ( $\alpha$ -spectrin) is a known substrate of caspase-3 as well as calpains. Although caspases and calpains share a number of substrates, their cleavage during treatment with RES in MCF-7 cells would indicate calpain activity because effector caspases are not activated in this model. Over a period of 24 to 48h in the presence of RES specific calpain-dependent processing of fodrin was detected, evidenced by disappearance of the 240/280 kD native band. However, in the presence of RES and the calpain inhibitor SJA6017, the native fodrin remains intact at all times and the 145/150 kD cleavage was not observed (Fig 6B; top panel). As expected, no caspase-3-mediated 120 kD breakdown product was observed. Mechanisms that regulate the cellular extrusion of  $\text{Ca}^{2+}$  could potentially rectify the RES-induced  $\text{Ca}^{2+}$  increase. To determine whether RES activated calpain can target such a mechanism, we explored the cleavage pattern of  $\text{Ca}^{2+}$  pumps in the presence of a known calpain inhibitor. Beginning at 24 h after RES treatment native PMCA1a/b (130-134 kD) was cleaved in a calpain-dependent manner in MCF-7 cells (Fig. 6B; middle panel). Co-treating cells with the calpain inhibitor SJA6017 in the presence of RES prevented PMCA1a/b cleavage. However, there was no evidence of calpain-dependent PMCA4 degradation in the presence of RES (data not shown).

## Discussion

In search for novel strategies for further management of breast cancer, we have attempted to identify the molecular mechanisms involved in RES-induced apoptosis, both caspase-dependent and caspase-independent. To the best of our knowledge, this is one of the first studies to describe the chemotherapeutic effects of RES-induced alterations in  $\text{Ca}^{2+}$  homeostasis.

In the present study, we illustrate the *in vivo* anticancer efficacy of RES against breast cancer tumor growth in the MDA-MB-231 xenograft model without any toxicity. Data from preliminary studies suggests that RES exhibits similar efficacy against the MCF-7 xenograft model. *In vitro* studies demonstrate that RES exerts dose- and time-dependent anti-proliferative and pro-apoptotic effects in MCF-7 and MDA-MB-231 cells, thus decreasing cell viability. The antiproliferative activity of RES against tumor cell lines of different origins has been extensively characterized and attributed to inhibition of various factors like cyclooxygenase-1 and -2, ribonucleotide reductase, nuclear transcription factor-kappa B (NF- $\kappa$ B) and its target genes (Aggarwal, et al., 2004; Delmas, et al., 2006). In contrast to *in vitro* data on enzyme inhibition, the RES anticancer effect *in vivo* may involve deregulation of multiple targets, promoting parallel or overlapping cascades of events inducing cell cycle arrest and eventually apoptosis.

Although RES has been shown to instigate apoptosis in various cancer models, data from our studies show that mitochondria were significantly affected shortly after RES treatment and likely play a central role in mediating apoptosis. RES treatment rapidly dissipates  $\Delta\Psi_m$  in whole cells and lower concentrations of RES were sufficient to influence a loss of  $\Delta\Psi_m$  in isolated mitochondria, indicating the possibility of a novel



RES target protein in the mitochondria. Opening of the mPTP comprised of the adenine-nucleotide translocator (ANT) and the voltage-dependent anion channel (VDAC) have been suggested to play important roles in mediating loss of  $\Delta\Psi_m$  and cyt *c* release (Martinou, et al., 2000; Petronilli, et al., 2001). Whether resveratrol's ability to directly target mitochondria and cause a loss of  $\Delta\Psi_m$  in breast cancer cells are somehow linked through these protein complexes requires further investigation.

Disruption of  $\Delta\Psi_m$  leading to mitochondrial permeabilization commonly accompanies or precedes release of cyt *c* and Smac/DIABLO into the cytoplasm, leading to formation of an active apoptosome complex, activation of caspase-9, which then activates the executioner caspase-3 to orchestrate apoptosis (Green, 2005). We demonstrate that RES triggered release of cyt *c* and Smac/DIABLO from mitochondria of MDA-MB-231 cells, which precedes the activation of caspases-9 and -3, confirming previous findings from other groups in tumor cell lines of different origins (Aggarwal, et al., 2004; Jiang, et al., 2005; Pozo-Guisado, et al., 2005). Although the precise mechanism that mediates the release of cyt *c* and Smac/DIABLO from the mitochondria is unclear, apoptosis-associated mitochondrial events induced by RES in many cancer cell types have been shown to be facilitated by the altered expression and mitochondrial localization of apoptotic regulators, such as down-modulation of the anti-apoptotic proteins Bcl-2 and Bcl-X<sub>L</sub>, and the up-regulation and mitochondrial translocation of pro-apoptotic Bax and Bak (Jiang, et al., 2005; Mahyar-Roemer, et al., 2002; Pozo-Guisado, et al., 2005). As anticipated, activation of caspase-9 and -3 was not detectable upon RES treatment of MCF-7 cells. Alternatively, extrinsic death receptor mediated apoptosis proceeding through the activation of initiator caspases-2 and -8 has been elicited by RES (Delmas,

et al., 2003; Mohan, et al., 2006). However, the absence of caspase-2 and -8 activation in response to RES treatment of MDA-MB-231 and MCF-7 cells indicates that the death receptor pathway is not a likely early mechanism of RES-induced apoptosis in these cells.

Our results reveal that RES evokes a rapid and biphasic increase in  $[Ca^{2+}]_i$  in both breast cancer cell lines, supporting our hypothesis that homeostatic mechanisms for regulating cellular  $Ca^{2+}$  possibly play a central role during RES-induced apoptosis. The initial rise appears to be dependent upon the ability of RES to stimulate the TG-sensitive  $Ca^{2+}$  stores, likely the ER. The second rise is possibly due to the release of buffered  $Ca^{2+}$  from the mitochondrial stores or extracellular influx of  $Ca^{2+}$  by plasma membrane channels. To confirm the source of this RES-induced  $Ca^{2+}$  release organelle-specific  $Ca^{2+}$ -sensitive indicators need to be employed.

During apoptosis the amplitude of the initial  $[Ca^{2+}]_i$  elevation is usually within the range of non-lethal stimulations, while the subsequent rise leading to a massive  $Ca^{2+}$  accumulation requires additional mechanisms to terminally deregulate cellular  $Ca^{2+}$  handling (Orrenius, et al., 2003). Our results demonstrate for the first time that RES treatment induces calpain activation in MCF-7 cells, which can be blocked by active-site calpain inhibitors and BAPTA-AM. Because no difference in the substrate specificity of the calpain isozymes has been found, considering the level of RES-induced elevation in  $[Ca^{2+}]_i$  we conclude that RES at least activated  $\mu$ -calpain and possibly also other calpains. In the present study, activated calpain targets cytoskeletal proteins such as fodrin and the high affinity  $Ca^{2+}$  pump, PMCA1, for degradation in cells exposed to RES. The calpain-dependent degradation of PMCA1 possibly prevents it from functioning and

maintaining  $\text{Ca}^{2+}$  homeostasis. This, in turn, could facilitate  $\text{Ca}^{2+}$  leakage down its concentration gradient into the cytosol, providing a secondary sustained  $\text{Ca}^{2+}$  elevation that results in proteolytic degradation and ultimately apoptosis. Co-administration of RES and calpain inhibitor successfully abrogates calpain-induced fodrin and PMCA1 cleavage. Previously, *in vitro* studies have shown PMCA1, 2, and 4 to be susceptible to calpain degradation with differing sensitivities, and the erythrocyte calcium pump has been shown to be a preferred substrate of calpain *in vivo* (Guerini, et al., 2003). To the best of our knowledge this is the first study demonstrating an *in vivo* calpain-induced cleavage of PMCA1 in response to RES.

The mitochondria play an essential role in buffering physiological loads of  $\text{Ca}^{2+}$  upon insult, while the mPTP provides a fast  $\text{Ca}^{2+}$  extrusion mechanism in response to abnormally high levels of  $\text{Ca}^{2+}$  that accumulate in mitochondria during apoptosis. Recently, RES has been demonstrated to promote  $\text{Ca}^{2+}$ -mediated mPTP opening by activating a  $\text{Ca}^{2+}$ -induced  $\text{Ca}^{2+}$  release (CICR) from rat liver mitochondria, and this effect was completely inhibited by CsA (Tian, et al., 2006). Interestingly, we observed that RES-induced calpain activation was significantly inhibited in the presence of CsA, suggesting that calpain activation may be a post-mitochondrial event. The precise mechanism of this mPTP inhibition is still elusive, although it is possible that CsA enhances the mitochondrial uptake and retention of  $\text{Ca}^{2+}$  and thereby prevents calpain activation during recovery, as indicated in a recent study where CsA prevented calpain activation following microcystin-induced cell death in hepatocytes (Ding, et al., 2002).

These results support the hypothesis that RES is a multi-faceted molecule capable of directly targeting the mitochondria and activating the intrinsic mitochondrial caspase-

dependent form of apoptosis. In addition, RES targets the thapsigargin-sensitive ER  $\text{Ca}^{2+}$  stores to cause an elevation of intracellular  $\text{Ca}^{2+}$  levels in both breast cancer cell lines. Subsequent  $\text{Ca}^{2+}$ -dependent activation of calpain is observed. This mechanism of apoptosis may be especially relevant in tumors lacking caspase-3 activity (Devarajan, et al., 2002). Thus, it is likely that resveratrol's pro-apoptotic mechanism involves deregulation of multiple targets associated with the mitochondria and ER leading to activation of different enzymatic cascades described in Fig. 8.

Collectively, these data for the first time, link changes in  $\text{Ca}^{2+}$  homeostasis to the RES-mediated initiation of apoptosis. Sustained elevations in intracellular  $\text{Ca}^{2+}$ , therefore, might serve as a universal cell death signal that can be exploited for anti-tumor therapy. Differences in expression of a RES target and/or  $\text{Ca}^{2+}$  regulatory mechanisms in cancer versus normal cells may allow RES to induce apoptosis selectively in breast cancer cells. Identification of a putative RES mitochondrial and/or ER target could lead to the synthesis of more efficacious apoptotic anti-cancer agents. Our findings will hopefully aid in the development of therapeutic strategies for the further development of RES as a non-toxic alternative to conventional anticancer therapies for breast cancer.

## Acknowledgments

The authors would like to thank Joshua Harder for help in preparation of the manuscript and Dr. Mary J. Lindstrom for conducting the statistical analyses.

## References

- Aggarwal BB, Bhardwaj A, Aggarwal RS, Seeram NP, Shishodia S and Takada Y (2004) Role of resveratrol in prevention and therapy of cancer: preclinical and clinical studies. *Anticancer Res* **24**:2783-2840.
- Ashkenazi A and Dixit VM (1998) Death receptors: signaling and modulation. *Science* **281**:1305-1308.
- Banerjee S, Bueso-Ramos C and Aggarwal BB (2002) Suppression of 7,12-dimethylbenz(a)anthracene-induced mammary carcinogenesis in rats by resveratrol: role of nuclear factor-kappaB, cyclooxygenase 2, and matrix metalloprotease 9. *Cancer Res* **62**:4945-4954.
- Bano D, Young KW, Guerin CJ, Lefevre R, Rothwell NJ, Naldini L, Rizzuto R, Carafoli E and Nicotera P (2005) Cleavage of the plasma membrane Na<sup>+</sup>/Ca<sup>2+</sup> exchanger in excitotoxicity. *Cell* **120**:275-285.
- Bhat KP, Lantvit D, Christov K, Mehta RG, Moon RC and Pezzuto JM (2001) Estrogenic and antiestrogenic properties of resveratrol in mammary tumor models. *Cancer Res* **61**:7456-7463.
- Bradamante S, Barenghi L and Villa A (2004) Cardiovascular protective effects of resveratrol. *Cardiovasc Drug Rev* **22**:169-188.

Buluc M and Demirel-Yilmaz E (2006) Resveratrol decreases calcium sensitivity of vascular smooth muscle and enhances cytosolic calcium increase in endothelium.

*Vascul Pharmacol* **44**:231-237.

Delmas D, Lancon A, Colin D, Jannin B and Latruffe N (2006) Resveratrol as a chemopreventive agent: a promising molecule for fighting cancer. *Curr Drug Targets*

**7**:423-442.

Delmas D, Rebe C, Lacour S, Filomenko R, Athias A, Gambert P, Cherkaoui-Malki M, Jannin B, Dubrez-Daloz L, Latruffe N and Solary E (2003) Resveratrol-induced apoptosis is associated with Fas redistribution in the rafts and the formation of a death-inducing signaling complex in colon cancer cells. *J Biol Chem* **278**:41482-41490.

Devarajan E, Sahin AA, Chen JS, Krishnamurthy RR, Aggarwal N, Brun AM, Sapino A, Zhang F, Sharma D, Yang XH, Tora AD, Mehta K (2002) Down-regulation of caspase-3 in breast cancer: a possible mechanism for chemoresistance. *Oncogene* **21**:8843-8851.

Ding WX, Shen HM and Ong CN (2002) Calpain activation after mitochondrial permeability transition in microcystin-induced cell death in rat hepatocytes. *Biochem Biophys Res Commun* **291**:321-331.

Garvin S, Ollinger K and Dabrosin C (2006) Resveratrol induces apoptosis and inhibits angiogenesis in human breast cancer xenografts in vivo. *Cancer Lett* **231**:113-122.

Green DR (2005) Apoptotic pathways: ten minutes to dead. *Cell* **121**:671-674.

- Green DR and Reed JC (1998) Mitochondria and apoptosis. *Science* **281**:1309-1312.
- Grynkiewicz G, Poenie M and Tsien RY (1985) A new generation of Ca<sup>2+</sup> indicators with greatly improved fluorescence properties. *J Biol Chem* **260**:3440-3450.
- Guerini D, Pan B and Carafoli E (2003) Expression, purification, and characterization of isoform 1 of the plasma membrane Ca<sup>2+</sup> pump: focus on calpain sensitivity. *J Biol Chem* **278**:38141-38148.
- Guttmann RP and Johnson GV (1998) Oxidative stress inhibits calpain activity in situ. *J Biol Chem* **273**:13331-13338.
- Hambrock A, de Oliveira Franz CB, Hiller S, Grenz A, Ackermann S, Schulze DU, Drews G and Osswald H (2007) Resveratrol binds to the sulfonylurea receptor (SUR) and induces apoptosis in a SUR subtype-specific manner. *J Biol Chem* **282**:3347-3356.
- Harwood SM, Yaqoob MM and Allen DA (2005) Caspase and calpain function in cell death: bridging the gap between apoptosis and necrosis. *Ann Clin Biochem* **42**:415-431.
- Jang M, Cai L, Udeani GO, Slowing KV, Thomas CF, Beecher CW, Fong HH, Farnsworth NR, Kinghorn AD, Mehta RG, Moon RC and Pezzuto JM (1997) Cancer chemopreventive activity of resveratrol, a natural product derived from grapes. *Science* **275**:218-220.



Janicke RU, Sprengart ML, Wati MR and Porter AG (1998) Caspase-3 is required for DNA fragmentation and morphological changes associated with apoptosis. *J Biol Chem* **273**:9357-9360.

Jemal A, Siegel R, Ward E, Murray T, Xu J, Smigal C and Thun MJ (2006) Cancer statistics, 2006. *CA Cancer J Clin* **56**:106-130.

Jiang H, Zhang L, Kuo J, Kuo K, Gautam SC, Groc L, Rodriguez AI, Koubi D, Hunter TJ, Corcoran GB, Seidman MD and Levine RA (2005) Resveratrol-induced apoptotic death in human U251 glioma cells. *Mol Cancer Ther* **4**:554-561.

Kim YA, Choi BT, Lee YT, Park DI, Rhee SH, Park KY, Choi YH (2004) Resveratrol inhibits cell proliferation and induces apoptosis of human breast carcinoma MCF-7 cells. *Oncol Rep* **11**:441-6.

Lin HY, Lansing L, Merillon JM, Davis FB, Tang HY, Shih A, Vitrac X, Krisa S, Keating T, Cao HJ, Bergh J, Quackenbush S and Davis PJ (2006) Integrin alphaVbeta3 contains a receptor site for resveratrol. *FASEB J* **20**:1742-1744.

Liu X, Van Vleet T and Schnellmann RG (2004) The role of calpain in oncotic cell death. *Annu Rev Pharmacol Toxicol* **44**:349-370.

Mahyar-Roemer M, Kohler H and Roemer K (2002) Role of Bax in resveratrol-induced apoptosis of colorectal carcinoma cells. *BMC Cancer* **2**:27.

Martinou JC, Desagher S and Antonsson B (2000) Cytochrome c release from mitochondria: all or nothing. *Nat Cell Biol* **2**:E41-3.

- Mohan J, Gandhi AA, Bhavya BC, Rashmi R, Karunagaran D, Indu R and Santhoshkumar TR (2006) Caspase-2 triggers Bax-Bak-dependent and - independent cell death in colon cancer cells treated with resveratrol. *J Biol Chem* **281**:17599-17611.
- Montero M, Lobaton CD, Gutierrez-Fernandez S, Moreno A and Alvarez J (2004) Calcineurin-independent inhibition of mitochondrial Ca<sup>2+</sup> uptake by cyclosporin A. *Br J Pharmacol* **141**:263-268.
- Orrenius S, Zhivotovsky B and Nicotera P (2003) Regulation of cell death: the calcium-apoptosis link. *Nat Rev Mol Cell Biol* **4**:552-565.
- Petronilli V, Penzo D, Scorrano L, Bernardi P and Di Lisa F (2001) The mitochondrial permeability transition, release of cytochrome c and cell death. Correlation with the duration of pore openings in situ. *J Biol Chem* **276**:12030-12034.
- Potter DA, Tirnauer JS, Janssen R, Croall DE, Hughes CN, Fiacco KA, Mier JW, Maki M and Herman IM (1998) Calpain regulates actin remodeling during cell spreading. *J Cell Biol* **141**:647-662.
- Pozo-Guisado E, Merino JM, Mulero-Navarro S, Lorenzo-Benayas MJ, Centeno F, Alvarez-Barrientos A and Fernandez-Salguero PM (2005) Resveratrol-induced apoptosis in MCF-7 human breast cancer cells involves a caspase-independent mechanism with downregulation of Bcl-2 and NF-kappaB. *Int J Cancer* **115**:74-84.
- Robinson JA, Jenkins NS, Holman NA, Roberts-Thomson SJ and Monteith GR (2004) Ratiometric and nonratiometric Ca<sup>2+</sup> indicators for the assessment of intracellular

free  $\text{Ca}^{2+}$  in a breast cancer cell line using a fluorescence microplate reader. *J Biochem Biophys Methods* **58**:227-237.

Sareen D, van Ginkel PR, Takach JC, Mohiuddin A, Darjatmoko SR, Albert DM and Polans AS (2006) Mitochondria as the primary target of resveratrol-induced apoptosis in human retinoblastoma cells. *Invest Ophthalmol Vis Sci* **47**:3708-3716.

Sasaki T, Kikuchi T, Yumoto N, Yoshimura N and Murachi T (1984) Comparative specificity and kinetic studies on porcine calpain I and calpain II with naturally occurring peptides and synthetic fluorogenic substrates. *J Biol Chem* **259**:12489-12494.

Savouret JF and Quesne M (2002) Resveratrol and cancer: a review. *Biomed Pharmacother* **56**:84-87.

Sun XM, MacFarlane M, Zhuang J, Wolf BB, Green DR and Cohen GM (1999) Distinct caspase cascades are initiated in receptor-mediated and chemical-induced apoptosis. *J Biol Chem* **274**:5053-5060.

Tian XM, Ma XD and Yan F (2006) Resveratrol promotes  $\text{Ca}^{2+}$ -induced  $\text{Ca}^{2+}$  release from rat liver cell mitochondria mediated by  $\text{Ca}^{2+}$ . *Nan Fang Yi Ke Da Xue Xue Bao* **26**:910-913.

## Footnotes

\*This work was supported by NIH grant RO1CA103653 (to A.S.P.), and grants from the Retina Research Foundation (to A.S.P.), the Mandelbaum Cancer Therapeutics Initiative (to A.S.P. and D.M.A.), and NIH core grant P30 EY016665-02.

<sup>1</sup>Send reprint requests to:

Dr. Arthur S. Polans

Department of Ophthalmology and Visual Sciences,

Rm. K6/466 Clinical Sciences Center,

600 Highland Avenue, Madison, WI – 53792.

Phone: (608) 265-4423; Fax: (608) 265-6021

E-mail: [aspolans@wisc.edu](mailto:aspolans@wisc.edu).

## Figure Legends

**Table 1: Oral administration of resveratrol suppresses growth of an established MDA-MB-231 breast cancer xenograft *in vivo*.** MDA-MB-231 cells resuspended in Matrigel were injected subcutaneously into the dorsal flank of *nu/nu* mice and tumors allowed to grow. Thirty-six mice per group were fed RES (50 mg/kg per day) in vehicle (Neobee M5 oil) or vehicle alone by oral gavage. At the end of 5 weeks of treatment tumors were recovered and measured. Tumor volume was transformed to the log scale before analysis to obtain approximately normal distribution residuals and analyzed using a 1-way analysis of variance (ANOVA) test to detect statistical differences in tumor size among the groups. Data represent the average tumor volume in mm<sup>3</sup> assessed by caliper measurement  $\pm$  standard error. Differences in tumor volume among the vehicle and RES treated groups were considered statistically significant at  $p < 0.05$ .

**Fig. 1: Resveratrol engenders concentration- and time-dependent anti-proliferation and apoptosis in breast cancer cells *in vitro*.** **A**, cells were seeded at a density of  $2.5 \times 10^4/200 \mu\text{l}$  in a 96-well plate and treated with DMSO vehicle control (UNT) or 25, 50, 100 and 200  $\mu\text{M}$  RES. Cell viability was measured using the CellTiter-Blue™ assay at the end of 1, 3, 5 and 7 days of treatment as described in “Experimental Procedures”. **B**, cells seeded on 100 mm plates at a density of  $5 \times 10^6$  cells were treated with DMSO (UNT) or 50 and 100  $\mu\text{M}$  RES for 48 h. Nuclei were isolated from cells and stained with PI followed by flow cytometric analysis. The percentage of cells in G<sub>0</sub>/G<sub>1</sub>, S, and G<sub>2</sub>-M phases of the cell cycle were analyzed and represented within the histograms. **C**, cells were seeded at a density of  $2 \times 10^5$  cells/ml,

treated with DMSO vehicle (UNT) or 100  $\mu$ M RES for 24, 48, 72 or 96 h, stained with Hoechst 33528 and nuclear morphology examined by fluorescence microscopy. Cells exhibiting pyknotic nuclei and chromatin condensation were counted and the number of apoptotic cells determined as a percentage of the total number of cells in a viewing field. Value at each time point was averaged over five different viewing fields. Data (**A**, **B**, and **C**) represent means  $\pm$  SD of triplicate samples. Results are representative of one of three independent experiments with similar results.

**Fig. 2: Resveratrol causes loss of  $\Delta\Psi_m$  in intact cells and isolated mitochondria.**

**A**, MDA-MB-231 cells, and **B**, MCF-7 cells were treated with DMSO (UNT) or 50, 100, and 200  $\mu$ M RES, and positive controls, 25  $\mu$ M FCCP and 10  $\mu$ M valinomycin for 10 min. Cells in a suspension at  $5 \times 10^5$  cells/ml were rinsed, stained with JC-1 dye, and monitored for changes in the red – green fluorescence ratio (red fluorescence derived from J-aggregates in the mitochondria – green fluorescence from monomeric JC-1 in the cytosol). **C** and **D**, Mitochondrial fractions were isolated from MDA-MB-231 (**C**) and MCF-7 (**D**) cells as described under “Experimental Procedures”. Protein concentrations were measured using the Bradford assay to determine equal amounts per sample. Isolated mitochondria were treated with DMSO (UNT) or 10 nM, 1  $\mu$ M, 5  $\mu$ M, 10  $\mu$ M, and 100  $\mu$ M RES, and positive controls, 0.5% Na-azide and 25  $\mu$ M FCCP for 10 min and stained with JC-1. Changes in  $\Delta\Psi_m$  were measured by monitoring JC-1 red fluorescence intensity; undetectable (UD). Data (**A**, **B**, **C**, and **D**) represent means  $\pm$  SD of duplicate samples. Results are representative of one of three independent experiments with similar results.

**Fig. 3: RES provokes mitochondrial release of cytochrome c and Smac/DIABLO in MDA-MB-231 cells.** Cells seeded on plates were treated with DMSO (UNT) or 100  $\mu$ M RES for 4, 12, 24 and 48 h, washed and permeabilized in 0.04% digitonin extraction buffer. Cytosolic fractions free of mitochondria were prepared by differential centrifugation as described under “Experimental Procedures”. Fifty- $\mu$ g of cytosolic fraction was processed for Western blotting, probed with antibody against cyt c (*top panel*) and Smac/DIABLO (*center panel*). GAPDH (*bottom panel*) immunostaining served as a loading control. Results are representative of one of two independent experiments with similar results.

**Fig. 4: Resveratrol induces caspase-dependent apoptosis in MDA-MB-231 cells and caspase-independent apoptosis in MCF-7 cells.** **A** and **B**, MDA-MB-231 and MCF-7 cultures were treated with DMSO (UNT) for 72 h or 100  $\mu$ M RES for 24, 48, and 72 h, lysed, and caspase-9 (**A**) and caspase-3 (**B**) activities were measured spectrofluorometrically using respective peptide substrates. The *graphs* show relative fluorescence intensity of free AFC (**A**) and AMC (**B**) released upon enzymatic activation. **C** and **D**, cells were treated with DMSO control, 100  $\mu$ M RES, 1  $\mu$ M TG, 1  $\mu$ M staurosporine (STS), or exposed to 200 J/m<sup>2</sup> UV, lysed, and caspase-2 (**C**) and caspase-8 (**D**) activities were measured 24 h later using fluorometric peptide substrates. The *graphs* show relative fluorescence intensity of free AFC released. The lysates were adjusted for equal protein concentrations using the Bradford assay. Data (**A**, **B**, **C**, and **D**) represent means  $\pm$  SD of duplicate samples. Results are representative of one of three independent experiments with similar results.

**Fig. 5: Resveratrol increases intracellular calcium levels in breast cancer cells.**

MCF-7 and MDA-MB-231 cells seeded at  $2 \times 10^5$  cells in 96-well plates were loaded with fura-2-AM. **A**, DMSO control (UNT), 100  $\mu$ M RES or 5  $\mu$ M ionomycin were added to MCF-7 cells after basal measurements were made on a spectrofluorometer. After drug addition, measurements were made every 60 s for 10 min. *Graph* depicts changes in  $[Ca^{2+}]_i$  at 6 min after drug addition by measuring the fluorescence intensity ratio ( $F^{340}/F^{380}$ ) of the  $Ca^{2+}$ -bound/  $Ca^{2+}$ -free fura-2. *Histograms* represent means  $\pm$  SD of triplicate samples and represent one of at least two independent experiments. **B**, live cell microscopy was performed in MCF-7 cells to observe alterations in intracellular  $Ca^{2+}$  **before** and **after** addition of 100  $\mu$ M RES. Cells representative of an average response of the entire population before and drug treatment were selected and shown as pseudocolored ROI images, along with a reference pseudocolor scale depicting increasing  $[Ca^{2+}]_i$  concentration from *left to right*. **C**, **D**, and **E**, live cell microscopy was performed in MDA-MB-231 cells to measure changes in  $[Ca^{2+}]_i$  in response to 100  $\mu$ M RES and 5  $\mu$ M TG. The *number* in the *bottom right corner* of each fluorescent pseudocolored image represents the time in seconds after drug addition (**C** and **D**). The inset images (**C**) depict a cell with a maximal response in  $[Ca^{2+}]_i$  to RES treatment. The  $Ca^{2+}$  mobilization responses to RES (**C**) and TG (**D**) are also displayed in *graphs* showing changes in  $[Ca^{2+}]_i$  concentration (nM) after the measured  $F^{340}/F^{380}$  ratio was calibrated with standard solutions to make the required conversions. The *line segment* on top of the *graph* depicts the period of drug stimulation. Each *trace* represents the change in  $[Ca^{2+}]_i$  of an individual ROI (2 – 4 cells) selected over time; each *graph* is



representative of one of at least three independent experiments. **E; top left**, representative  $\text{Ca}^{2+}$  mobilization traces upon sequential exposure of cells to 5  $\mu\text{M}$  TG and 100  $\mu\text{M}$  RES. **E; bottom left**, change in  $[\text{Ca}^{2+}]_i$  upon addition of 100  $\mu\text{M}$  RES followed by 5  $\mu\text{M}$  TG exposure after near saturation of the biphasic RES response. **E; top right**, a trace of the cells treated with DMSO vehicle control. **E; bottom right**, 20  $\mu\text{M}$  BAPTA-AM was co-loaded with fura-2-AM and the  $\text{Ca}^{2+}$  mobilization response was measured in response to 100  $\mu\text{M}$  RES treatment.

**Fig. 6: Resveratrol activates calpain as a function of mPTP opening in MCF-7**

**cells. A**, MCF-7 cells were harvested and washed. For each condition,  $2.5 \times 10^5$  cells/ml were left untreated, or pre-treated with intracellular  $\text{Ca}^{2+}$ -chelator BAPTA-AM, and calpain inhibitors, PD150606, SJA6017, and MDL 28170 for 30-60 min. DMSO or 100  $\mu\text{M}$  RES was added to untreated or pre-treated cell suspension followed by the fluorogenic calpain substrate, S-LLVY-AMC. Subsequently, calpain activity was monitored as a function of time by measuring the increase in fluorescence intensity of free AMC using a spectrofluorometer. The graph depicts calpain activity curves for different conditions plotted at 15 min post-drug treatment. **B**, MCF-7 cells prepared and assayed for calpain activity described in **A**. Cells were left untreated or pre-treated with the mPTP inhibitor, CsA for 30-45 min. Cells were then treated with DMSO or RES followed by substrate addition. Free AMC fluorescence generated was measured and curves plotted at 15 min post treatment. Data (**A** and **B**) depict a representative curve obtained from duplicate points measured for each condition. The experiment was repeated three times with similar results.

**Fig. 7: Resveratrol induces degradation of calpain-specific protein substrates in MCF-7 cells.** Cells seeded on plates were treated with DMSO (UNT) or 100  $\mu$ M RES alone or in combination with the calpain inhibitor SJA6017 for a period of 24 and 48 h. Cultures were scraped, washed, lysed and protein concentration was determined in cell lysates using the Bradford assay. Twenty five- $\mu$ g protein was processed for Western blotting and probed with antibodies specific for  $\alpha$ -fodrin or PMCA1. GAPDH immunostaining served as a loading control. The experiments were repeated three times with similar results.

**Fig. 8: Mechanisms of resveratrol-induced apoptosis.** **1**, RES targets the mitochondria resulting in mitochondrial depolarization that is frequently associated with mPTP opening. Subsequent mitochondrial release of cyt *c* and Smac/DIABLO leads to activation of caspase-9 and caspase-3 resulting in apoptosis. **2**, RES targets the ER causing an elevation of  $[Ca^{2+}]_i$  that is biphasic in nature. The initial rise in cytoplasmic  $Ca^{2+}$  is probably buffered by the mitochondria. The second phase is likely due to the release of buffered mitochondrial  $Ca^{2+}$  to the cytoplasm, commonly known as  $Ca^{2+}$ -induced  $Ca^{2+}$  release (CICR). There is evidence that CICR can either precede or follow mitochondrial depolarization. Subsequent calpain activation may be the result of the first (*dotted arrow*) or second phase of rise in  $[Ca^{2+}]_i$ . Active calpain is responsible for proteolysis of its substrates, ultimately leading to apoptosis.

Table 1

Group	Tumor size (mm <sup>3</sup> )	Standard Error	n	*p-value
vehicle	630.96	103.86	36	0.003
50 mg/kg RES	307.62	52.3	36	

Figure 1

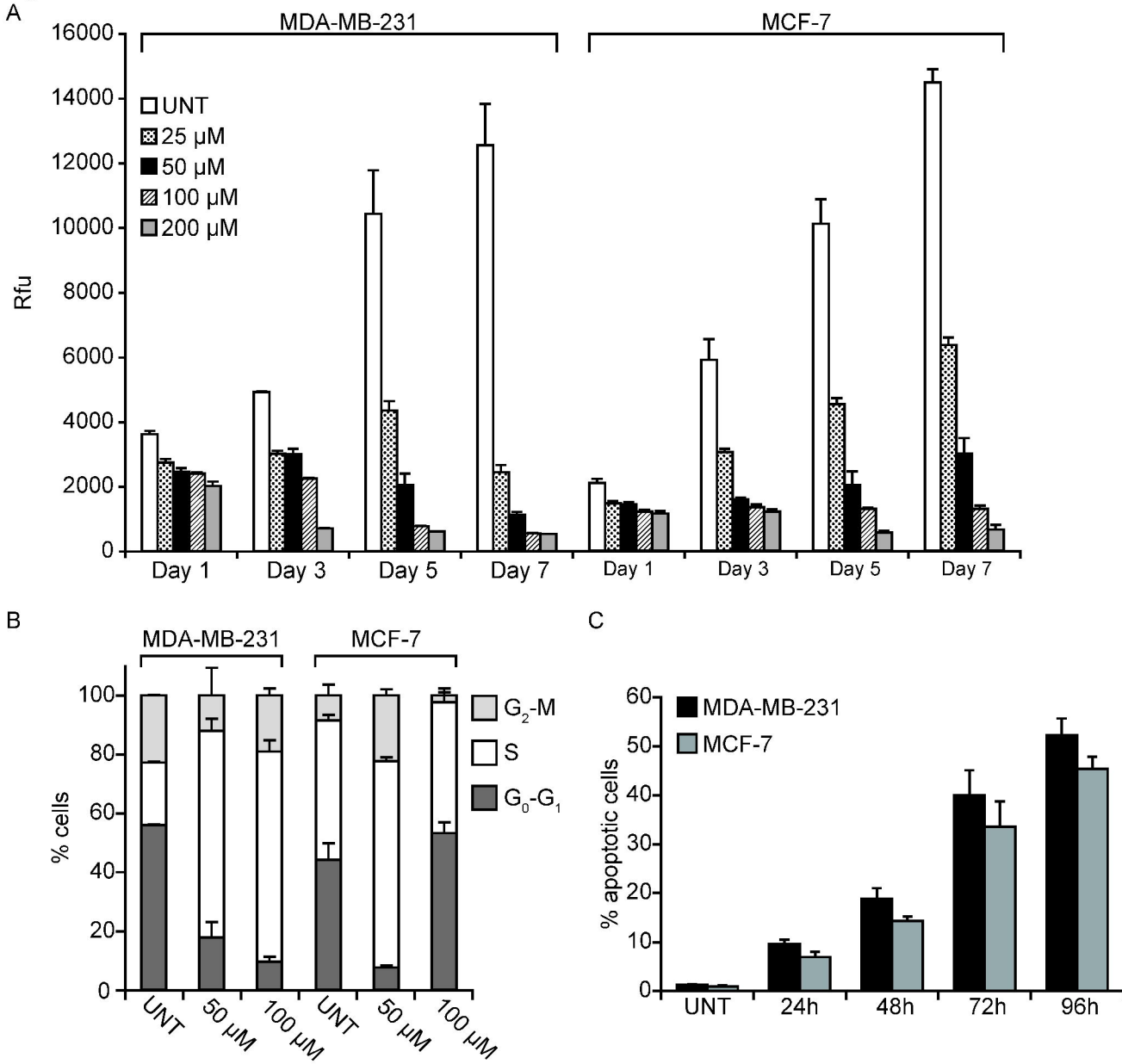


Figure 2

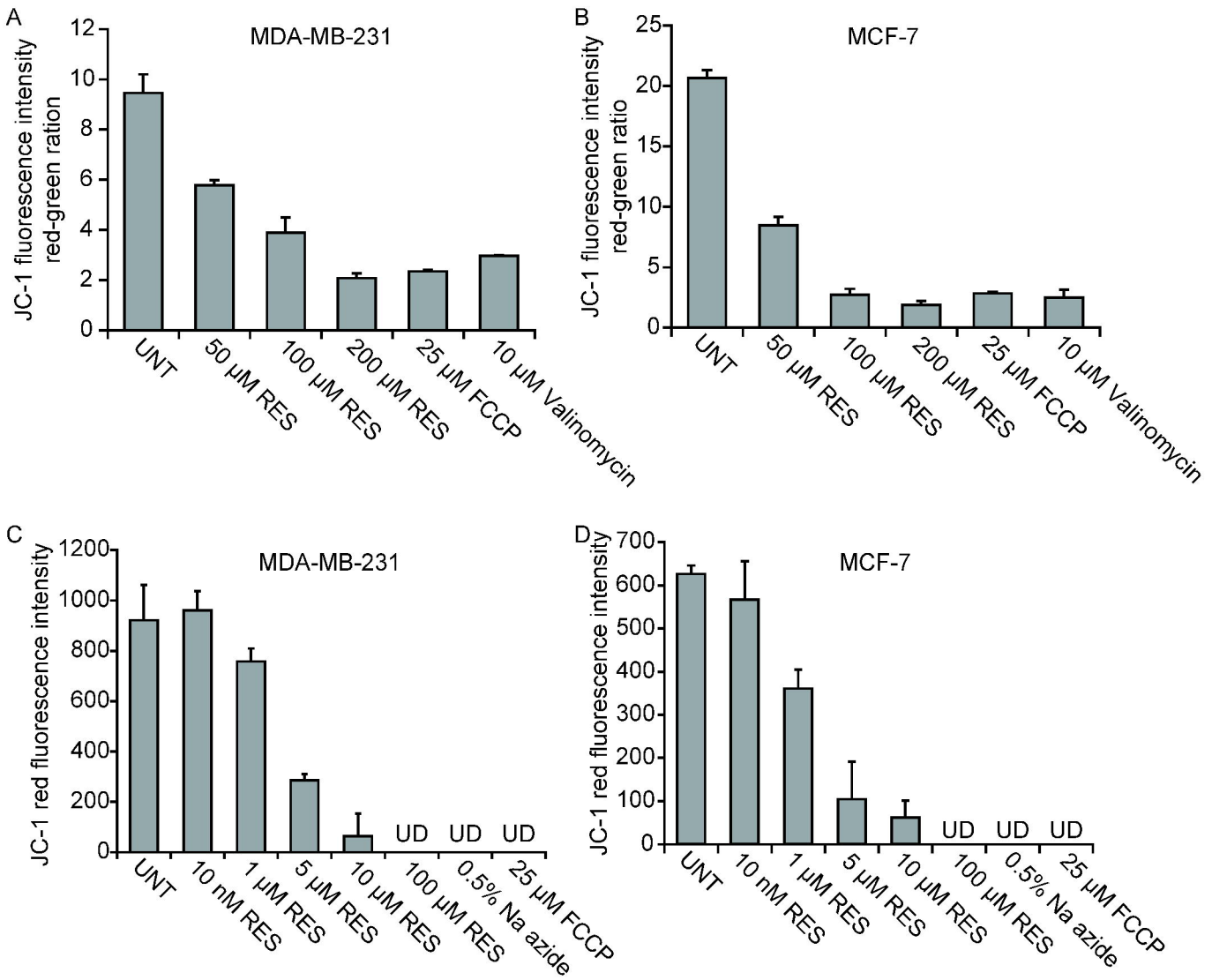


Figure 3

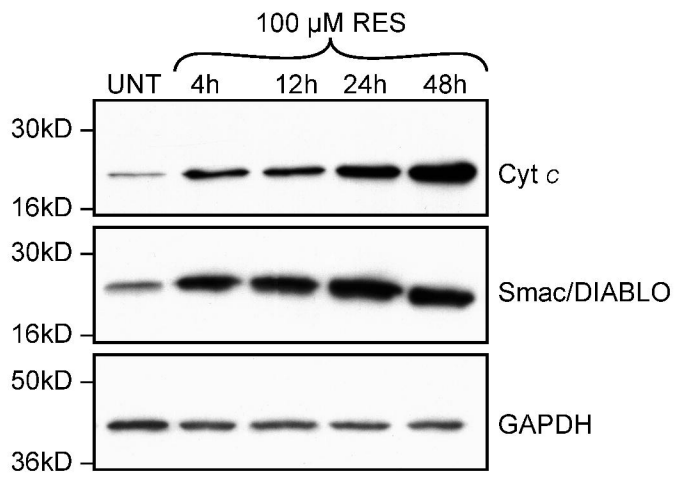


Figure 4

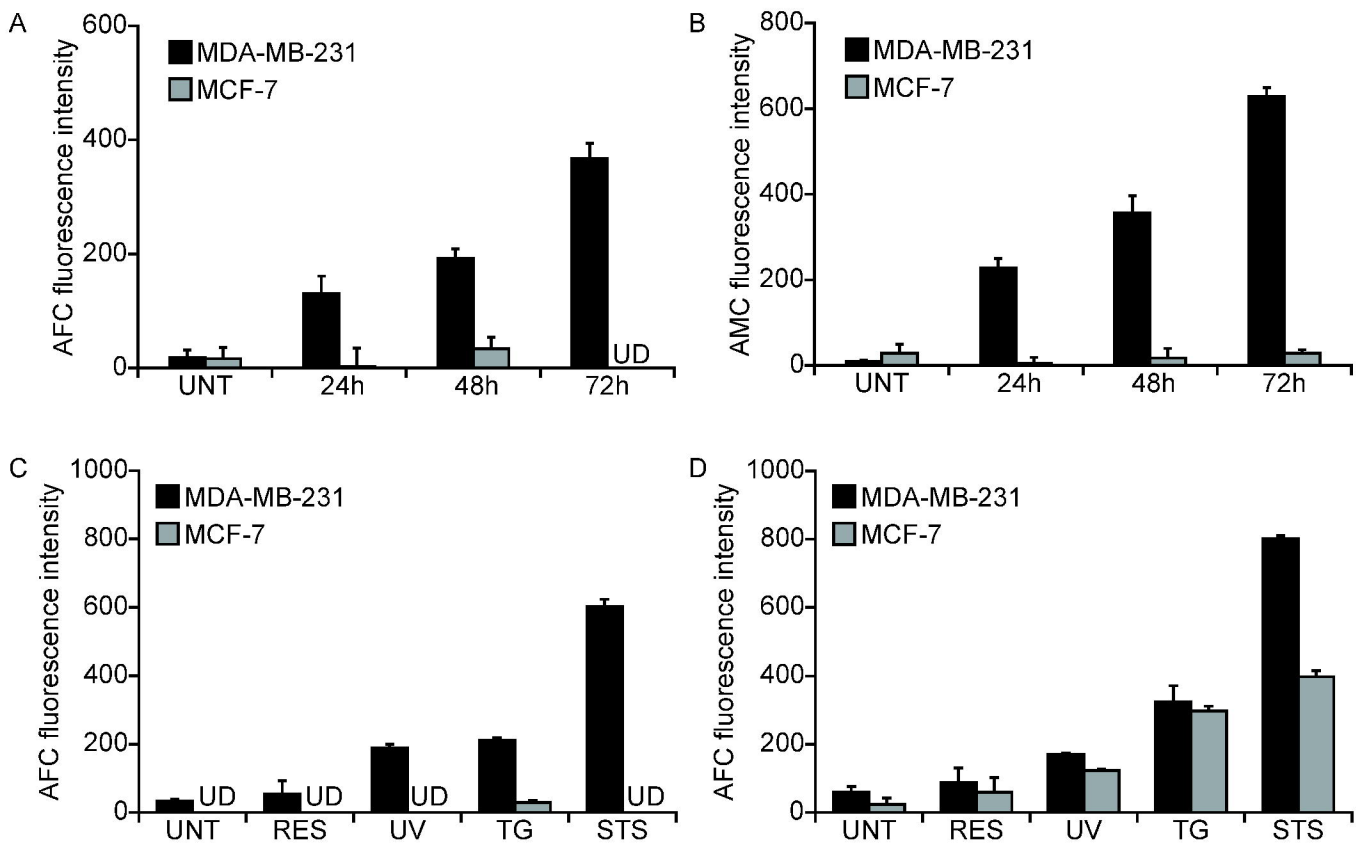


Figure 5

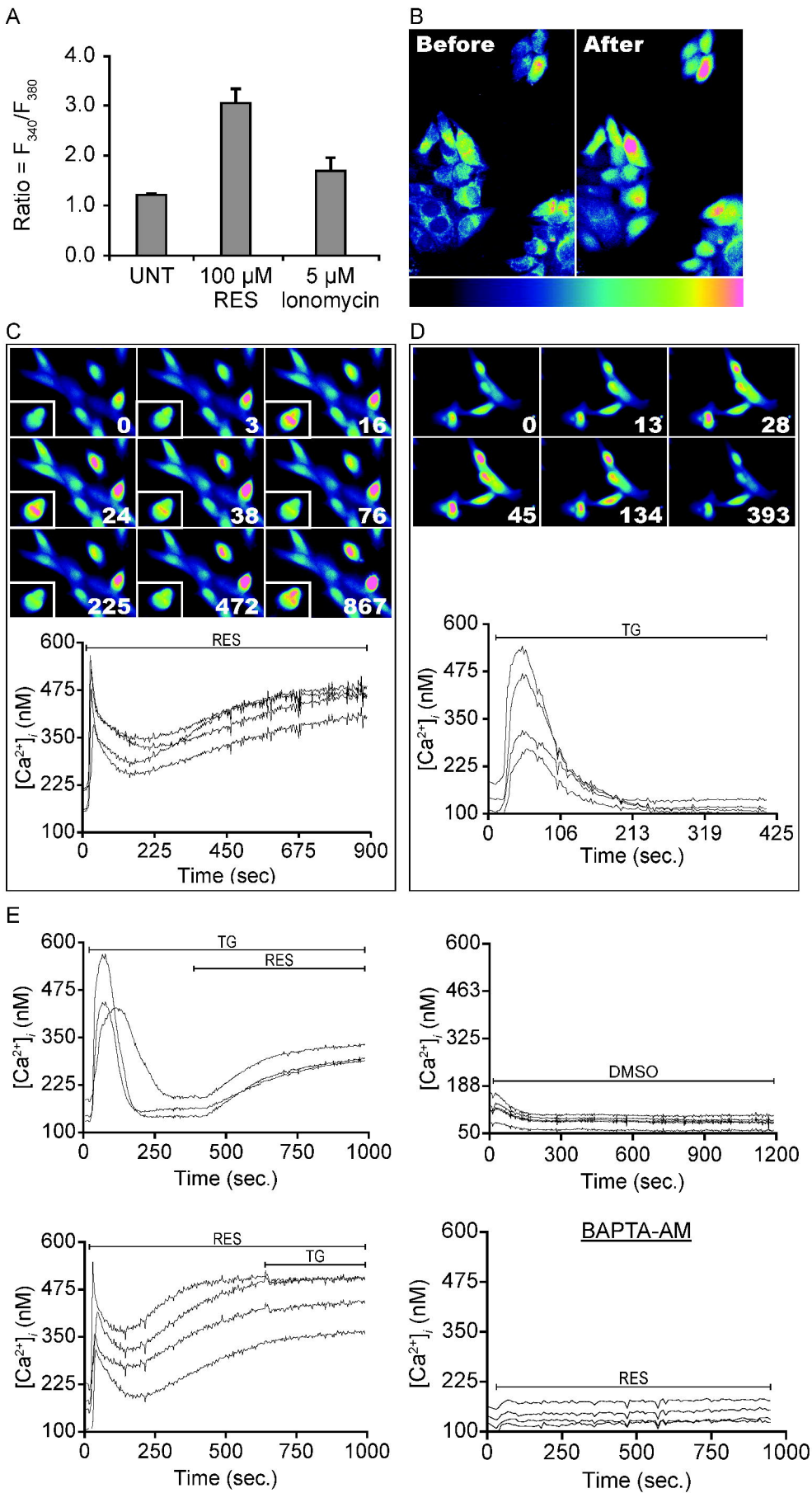
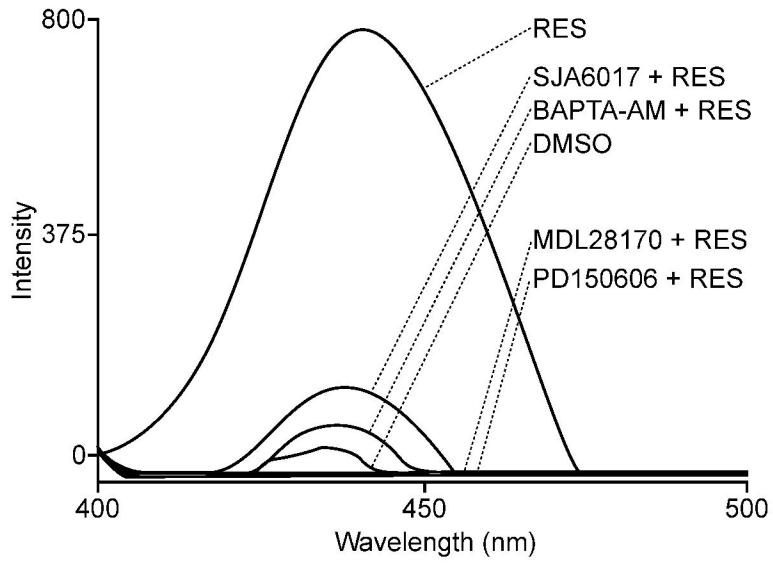




Figure 6

A



B

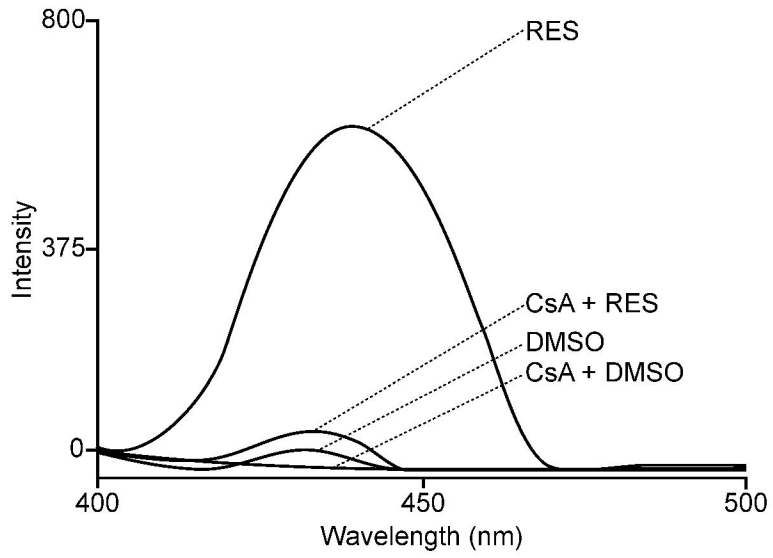


Figure 7

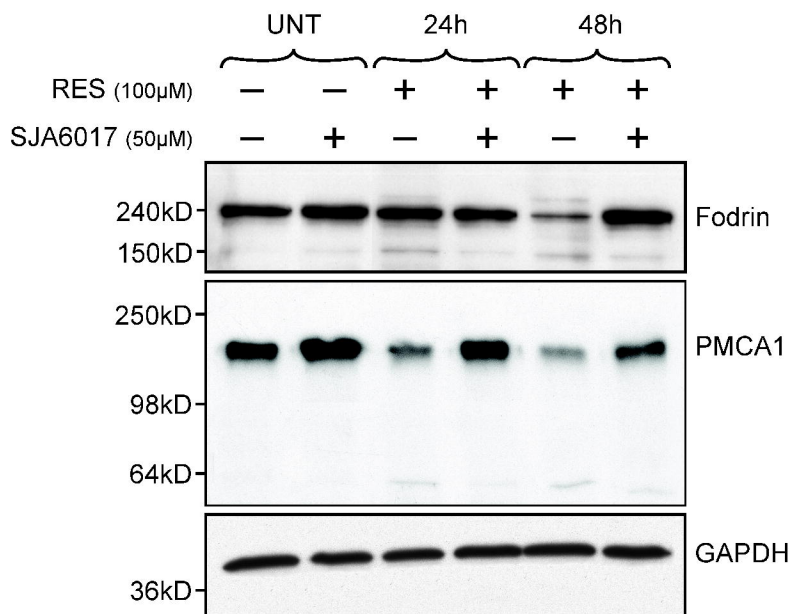


Figure 8

